Journal Name

ARTICLE

Controllable synthesis of lanthanide Yb^{3+} and Er^{3+} co-doped AWO_4 (A = Ca, Sr, Ba) micro-structured materials: phase, morphology and up-conversion luminescence enhancement

Received 00th January 20xx,
Accepted 00th January 20xx

DOI: 10.1039/x0xx00000x

www.rsc.org/

Jingbin Huang,[a,b] Qingfeng Li,[a,c] Jia Wang,[a,c] Lin Jin,[a,c] Boshi Tian,[a,c] Chunyang Li,[a,c] Yurong Shi, [a,c] Zhenling Wang*[a,c] and Jianhua Hao*[d]

Lanthanide ions (Yb^{3+}, Er^{3+}) co-doped AWO_4 (A = Ca, Sr, Ba) up-conversion (UC) luminescent materials have been synthesized using a hydrothermal method and characterized by various microstructural and optical techniques. The results indicate that AWO_4: Yb^{3+}, Er^{3+} samples have an identical body-centered tetragonal scheelite structure with different morphologies, including $CaWO_4$: Yb^{3+}, Er^{3+} microspheres, dumbbell-like $SrWO_4$: Yb^{3+}, Er^{3+} and bipyramid-like $BaWO_4$: Yb^{3+}, Er^{3+}. These samples exhibit visible emissions via UC process under near-infrared (NIR) light (980 nm) excitation. Interestingly, the UC luminescence properties of AWO_4: Yb^{3+}, Er^{3+} can be prominently increased after combination with fluorescent carbon dots (CDs) to form CDs@AWO_4: Yb^{3+}, Er^{3+} composites. Compared to the corresponding samples without combination with CDs, the UC emission intensities of CDs@$CaWO_4$: Yb^{3+}, Er^{3+}, CDs@$SrWO_4$: Yb^{3+}, Er^{3+} and CDs@$BaWO_4$: Yb^{3+}, Er^{3+} composites increase about three, six and seven folds in green emission area, and two, three and four folds in red emission area, respectively. The mechanism of UC luminescence enhancement is probably that the loss of non-radiative transitions from higher energy levels to the lower excited levels could be effectively reduced through the energy capture by CDs energy levels. The fluorescence enhancement for Yb^{3+} and Er^{3+} co-doped AWO_4 through combinating with CDs provides a simple strategy for tungstate system and other UC luminescent host systems.

1. Introduction

Up-conversion (UC) luminescent materials have the unique capability to generate ultraviolet, visible or near-infrared emissions due to the special configuration of 4f electrons in rare-earth elements under continuous-wave NIR light excitation.[1] Based on this special luminescent property, UC luminescent materials have attracted a great deal of attention due to their potential applications in a number of diverse fields such as lasers, optoelectronic devices, displays, bio-detection, bio-imaging and so forth.[2-4] It is well-known that ideal UC luminescent host materials should possess low lattice phonon energy, which is an essential requirement to maximize the radiative emission and minimize non-radiative losses.[2] According to the existing literatures, most of UC luminescent systems are based on fluoride hosts, such as $NaYF_4$,[5-10] LaF_3,[11] YF_3, [12,13] etc. The reason behind is that many fluoride hosts usually exhibit lower phonon energy (about 350 cm^{-1}) and higher chemical stability, which can increase the UC emission by hindering non-radiative relaxation losses.[14]

Compared with fluoride hosts, the phonon energy of AWO_4 (A = Ca, Sr, Ba) matrix is relatively high and generally larger than 500 cm^{-1} due to the stretching vibration of host lattices, which results in the lower UC luminescence efficiency when AWO_4 is used as UC luminescent host materials. However, as a self-activated luminescent material, AWO_4 (A = Ca, Sr, Ba) with scheelite-like structures represents an important family of oxides, and exhibits superior optical, photoelectronic and chemical stability performances. They have been used as host materials for a wide range of technologically significant applications, including phosphors, gas sensors, laser media, optical fibers and so on.[15–20] The previous works about rare-earth ions doped alkaline-earth-metal tungstates mainly focused on down-conversion (DC) luminescent materials, such as $CaWO_4$: Eu^{3+}/Tb^{3+}/Eu^{3+}, Tb^{3+},[21-26] $SrWO_4$: Eu^{3+},[27-29] $BaWO_4$: Eu^{3+}, etc.[30,31] As for Yb^{3+} and Er^{3+} co-doped AWO_4 UC luminescent materials, there are still very limited investigations. For instance, Xu et al. have synthesized Yb^{3+} and Er^{3+} co-doped $CaWO_4$ as an excellent optical thermometer.[32] Chai and co-workers have prepared Yb^{3+} and Er^{3+} co-doped $MgWO_4$ with bright dual-mode green emission and researched its temperature sensing properties.[33] Liu et al. synthesized $CaMo_xW_{1-x}O_4$: Yb^{3+}, Er^{3+} luminescent materials and explored the intensity changes of the upconversion luminescence before and after heat treatment.[34] It's well-known that the UC

[a] Henan Key Laboratory of Rare Earth Functional Materials; The Key Laboratory of Rare Earth Functional Materials and Applications, Zhoukou Normal University, Zhoukou 466001, P. R. China; *Email: zlwang2007@hotmail.com
[b] The College of Chemistry and Molecular Engineering, Zhengzhou University, Zhengzhou 450001, P. R. China
[c] International Joint Research Laboratory for Biomedical Nanomaterials of Henan, Zhoukou 466001, P. R. China
[d] Department of Applied Physics, The Hong Kong Polytechnic University, Hong Kong, P. R. China; *Email: jh.hao@polyu.edu.hk

Electronic Supplementary Information (ESI) available: TEM image, XRD pattern and luminescence photograph. See DOI: 10.1039/x0xx00000x

luminescence has relatively low luminescent quantum yield, which limits the further applications of these materials. Hence, it is necessary to develop a simple and feasible strategy to improve the UC luminescence performances. Recently, some attempts have been performed to improve UC luminescence efficiency, including tailoring the doping level and host lattices of UC nanoparticles,[6,35] forming core–shell structure,[36,37] using plasmon nanoantenna architecture, etc.[8–10] It is noticeable that formation of composite has proved to be an effective way for enhancing performance of the luminescent ions in phosphors.[38] However, to the best of our knowledge, it has been rarely reported to combine fluorescent CDs with the class of materials to form composite and therefore improve the luminescence properties of UC materials.

In this work, we report the synthesis of AWO_4: Yb^{3+}, Er^{3+} (A = Ca, Sr, Ba) UC luminescent materials with different morphologies (microsphere, dumbbell-like, bipyramid-like) through a hydrothermal process. The as-prepared samples exhibit UC luminescence (green and red emissions) under 980 nm NIR light excitation, and the emission intensity can be prominently enhanced through combination with fluorescence carbon dots (CDs) to form CDs@AWO_4: Yb^{3+}, Er^{3+} composites. The possible mechanism of UC luminescence enhancement for CDs@AWO_4: Yb^{3+}, Er^{3+} composites is discussed in detail. The luminescence enhancement strategy will provide a novel and feasible method to improve UC luminescence performance not only for tungstate host materials, but also for other host materials, such as phosphates, fluorides, vanadates, oxides, etc.

2. Experimental section

2.1. Preparation of AWO_4: Yb^{3+}, Er^{3+} (A = Ca, Sr, Ba) and combination with CDs

All chemicals employed were used directly without further purification. $Yb(NO_3)_3$ and $Er(NO_3)_3$ were prepared by dissolving the Yb_2O_3 (Analytical reagent, AR, 99.99%) and Er_2O_3 (AR, 99.99%) in diluted nitric acid, and the excess acid was evaporated by heating. In a typical synthesis, 1.0 mmol of nitrates containing $A(NO_3)_2{\cdot}xH_2O$ [$Ca(NO_3)_2{\cdot}4H_2O$ (AR, 99.0%), $Sr(NO_3)_2$ (AR, 99.5%), $Ba(NO_3)_2$ (AR, 99.8%)], $Yb(NO_3)_3$ and $Er(NO_3)_3$ with a constant molar ratio (A^{2+}: Yb^{3+}: Er^{3+} = 8.9: 1.0: 0.1) were dissolved in 10.0 mL of distilled water to form a clear solution, then 20.0 mL aqueous solution consisted of 1.0 mmol of $Na_2WO_4{\cdot}2H_2O$ (Chemical reagent, CR, 99.0%) was added into the above solution, and the mixture was continuously stirring for 10 min. Subsequently, the obtained suspension was transferred into a 50 mL Teflon-lined stainless autoclave, and heated at 180 ˚C for 12 h. After cooling to room temperature, the precipitates were collected by means of centrifugation, washed with distilled water and ethanol for several times, dried under air at 80 ˚C for 12 h, and finally obtained AWO_4: Yb^{3+}, Er^{3+} (A = Ca, Sr, Ba) samples.

For fabrication of CDs@AWO_4: Yb^{3+}, Er^{3+} (A = Ca, Sr, Ba) composites, the CDs were prepared according to a previous reported method, using citric acid as the carbon source in the presence of ethylenediamine.[39] The synthesis process of CDs@AWO_4: Yb^{3+}, Er^{3+} is similar to that of AWO_4: Yb^{3+}, Er^{3+}. Before the obtained suspension (the reaction mixture consists of $A(NO_3)_2{\cdot}xH_2O$, $Yb(NO_3)_3$, $Er(NO_3)_3$ and $Na_2WO_4{\cdot}2H_2O$) was transferred into a 50 mL of Teflon-lined stainless autoclave, a certain amount of CDs solution (about 0.25g/L) was added into the suspension and stirred for a given time, respectively. Then the mixtures containing CDs were transferred into a 50 mL of Teflon-lined stainless autoclave and hydrothermally treated, and the other procedure is similar to mentioned above.

2.2. Characterization

The crystal structures were identified by an Advance X-ray power diffraction (XRD, Bruker D8) at a scanning rate of 6°/min in the 2θ range from 10° to 80°, with Cu Kα radiation (λ = 0.15406 nm), keeping accelerating voltage and emission current at 40 kV and 40 mA, respectively. The morphology of the obtained samples was investigated by scanning electron microscopy (SEM, FEI Quanta 200) with an acceleration voltage of 25 kV and transmission electron microscope (TEM, JEOL-2100) with an acceleration voltage of 200 kV. X-ray photoelectron spectroscopy (XPS) measurements were observed using a Thermo Scientific Escalab 250 spectrometer (Escalab 250Xi) operated at 120 W. PL spectra were recorded using an Edinburgh Analytical Instrument apparatus (FLS920P) equipped with a 450 W xenon lamp and a 980 nm laser diode as the excitation sources, respectively.

3. Results and discussion

3.1. Phase structure and morphology of Yb^{3+} and Er^{3+} co-doped AWO_4 (A = Ca, Sr, Ba)

The crystal structures of the as-prepared Yb^{3+} and Er^{3+} co-doped AWO_4 (A = Ca, Sr, Ba) samples were characterized by XRD, as shown in Fig. 1. All diffraction peaks of the as-prepared

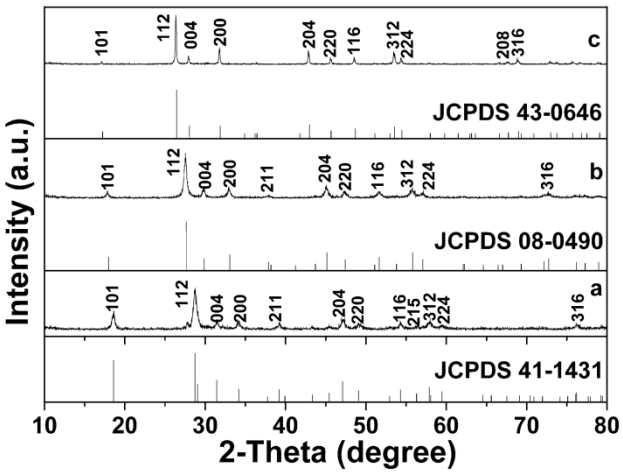

Fig. 1 XRD patterns of (a) $CaWO_4$: Yb^{3+}, Er^{3+}, (b) $SrWO_4$: Yb^{3+}, Er^{3+}, (c) $BaWO_4$: Yb^{3+}, Er^{3+} and the corresponding standard data for bulk $CaWO_4$ (JCPDS No. 41–1431), $SrWO_4$ (JCPDS No. 08–0490) and $BaWO_4$ (JCPDS No. 43–0646) powders.

Yb^{3+} and Er^{3+} co-doped $CaWO_4$, $SrWO_4$ and $BaWO_4$ samples (Fig. 1a, b, c) can be ascribed to a pure body-centered tetragonal

phase of bulk $CaWO_4$ (JCPDS No. 41–1431), $SrWO_4$ (JCPDS No. 08–0490) and $BaWO_4$ (JCPDS No. 43–0646), respectively. There is no other impurity peaks in the XRD patterns of Yb^{3+} and Er^{3+} co-doped AWO_4 (A = Ca, Sr, Ba) samples, indicating that the doped Er^{3+} and Yb^{3+} ions can be diffused into the AWO_4 host lattices. AWO_4 belongs to scheelite structure and has tetragonal phase with space group $I4_1/a$ and point group symmetry C_{4h}.[40] In this scheelite structure, the W^{6+} ions are within tetrahedral O–ion cages consisted of four oxygen atoms and isolated from each other and the A^{2+} ions are surrounded by eight oxygen atoms in the form of tetrahedral and dodecahedra, respectively.[41, 42] The site symmetry of A^{2+}, W^{6+} and O^{2-} ion is S_4, T_d and C_1, respectively.[43] When Yb^{3+} and Er^{3+} ions were doped into the AWO_4 hosts, since the ionic radius of Yb^{3+} (0.0985 nm) and Er^{3+} (0.1004 nm) are slightly smaller than that of Ca^{2+} (0.112 nm), Sr^{2+} (0.126 nm) and Ba^{2+} (0.142 nm) with eight coordination number, they could adapt to the S_4 site symmetry environments of A^{2+} ions and occupy the A^{2+} site in AWO_4 host lattice. Thus, trivalent lanthanide ions (Yb^{3+}, Er^{3+}) provide a particularly favorable situation for substitution in A^{2+} sites with isostructural replacement.[44]

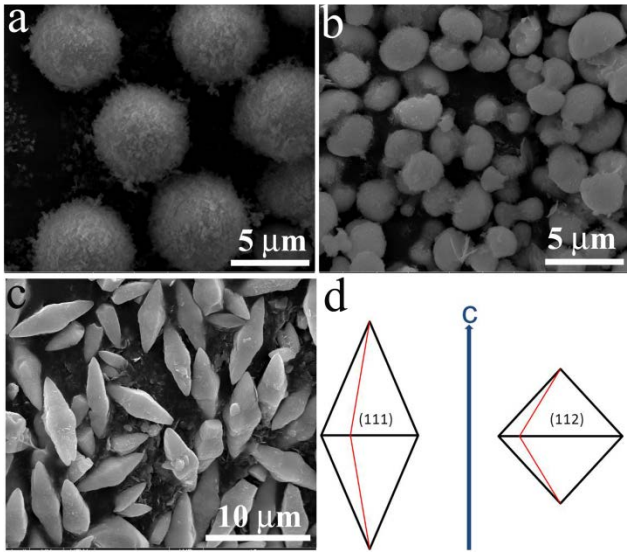

Fig. 2 SEM images of (a) $CaWO_4$: Yb^{3+}, Er^{3+}, (b) $SrWO_4$: Yb^{3+}, Er^{3+}, (c) $BaWO_4$: Yb^{3+}, Er^{3+} and (d) a schematic illustration of bipyramidal $BaWO_4$: Yb^{3+}, Er^{3+}.

Fig. 2 shows the representative SEM images of AWO_4: Yb^{3+}, Er^{3+} (A = Ca, Sr, Ba) samples. It can be seen from Fig. 2a that $CaWO_4$: Yb^{3+}, Er^{3+} samples are composed of homogeneous microspheres with an average diameter of about 6 μm. In order to clearly observe the surface microstructure of $CaWO_4$: Yb^{3+}, Er^{3+} microspheres, the low-magnification TEM image (Fig. 3a) displays a single $CaWO_4$: Yb^{3+}, Er^{3+} microsphere and there are many floccules on the surface of microsphere. The high-magnification TEM image (Fig. 3b) taken at a border of this microsphere (marked by red oval in Fig. 3a) indicates that these floccules on the surface of the microsphere are composed of lots of nanosheets with the thickness of about 30 nm, and these nanosheets are disorderly arranged on the surface of the $CaWO_4$: Yb^{3+},Er^{3+} microspheres. The SEM image of $SrWO_4$: Yb^{3+}, Er^{3+} (Fig. 2b) shows a dumbbell-like morphology with a short axis, and the average size is about 4 μm. The TEM images (Fig. 3c, d) show that the dumbbell-like morphology has smooth surface, and the width of pileus and length of axis are about 3.1 μm and 0.62 μm, respectively. The $BaWO_4$: Yb^{3+}, Er^{3+} sample has bipyramidal morphology, as shown in Fig. 2c. The well-defined bipyramidal morphology is characteristic of single-crystalline tetragonal $BaWO_4$ crystals bound by 8 planes of {11*l*}, such as {111} and {112}, and elongated along the c axis,[45] as shown in the schematic diagram (Fig. 2d). The corresponding TEM images are shown in Fig. 3e and f, and it also indicates that the surface of these $BaWO_4$: Yb^{3+}, Er^{3+} bipyramids are relatively smooth.

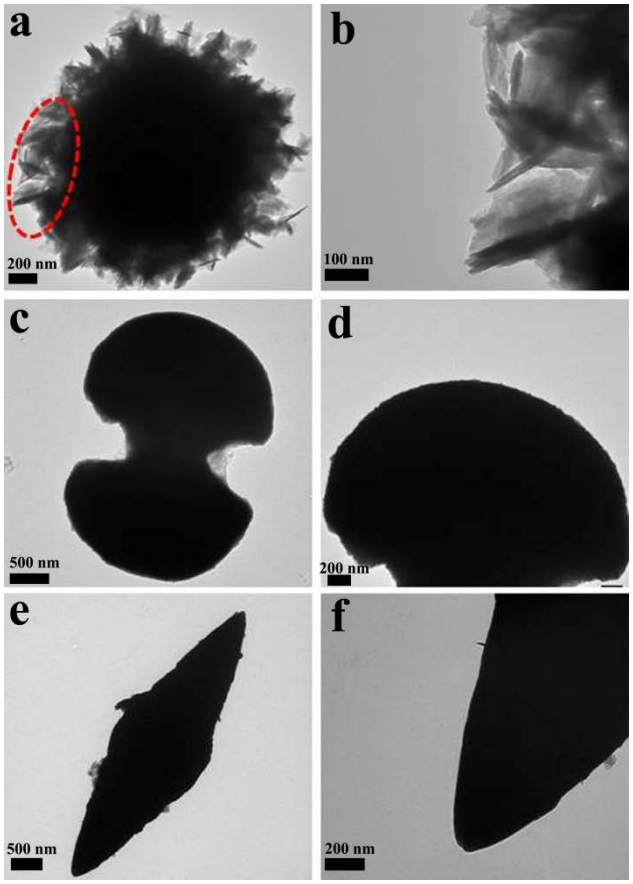

Fig. 3 Low- and high-magnification TEM images of (a, b) $CaWO_4$: Yb^{3+}, Er^{3+}, (c, d) $SrWO_4$: Yb^{3+}, Er^{3+} and (e, f) $BaWO_4$: Yb^{3+}, Er^{3+}.

3.2. CDs@AWO_4: Yb^{3+}, Er^{3+} (A = Ca, Sr, Ba) composites

In order to explore a feasible strategy to improve the UC luminescent performance of AWO_4: Yb^{3+}, Er^{3+} samples, the fluorescent carbon dots (CDs) were combined with AWO_4: Yb^{3+}, Er^{3+} to form CDs@AWO_4: Yb^{3+}, Er^{3+} composites. The fluorescent CDs were prepared using citric acid and ethylenediamine as the raw materials, and the TEM image of the as-prepared CDs (Fig. S1) displays an uniform and good dispersed spherical particles, with the average diameter of 1–3 nm. After the CDs were combined with AWO_4: Yb^{3+}, Er^{3+} samples, the scheelite phase structure of the CDs@AWO_4: Yb^{3+}, Er^{3+} composites remains unchanged, as shown in Fig. S2. The SEM images of CDs@AWO_4: Yb^{3+}, Er^{3+} composites were given in Fig. 4, and it can be seen that

the morphologies of $CaWO_4$: Yb^{3+}, Er^{3+} microspheres, $SrWO_4$: Yb^{3+}, Er^{3+} dumbbells and $BaWO_4$: Yb^{3+}, Er^{3+} bipyramid are mainly remained after combined with CDs, while there are still some changes on the surface of these samples. CDs@$CaWO_4$: Yb^{3+}, Er^{3+} samples are

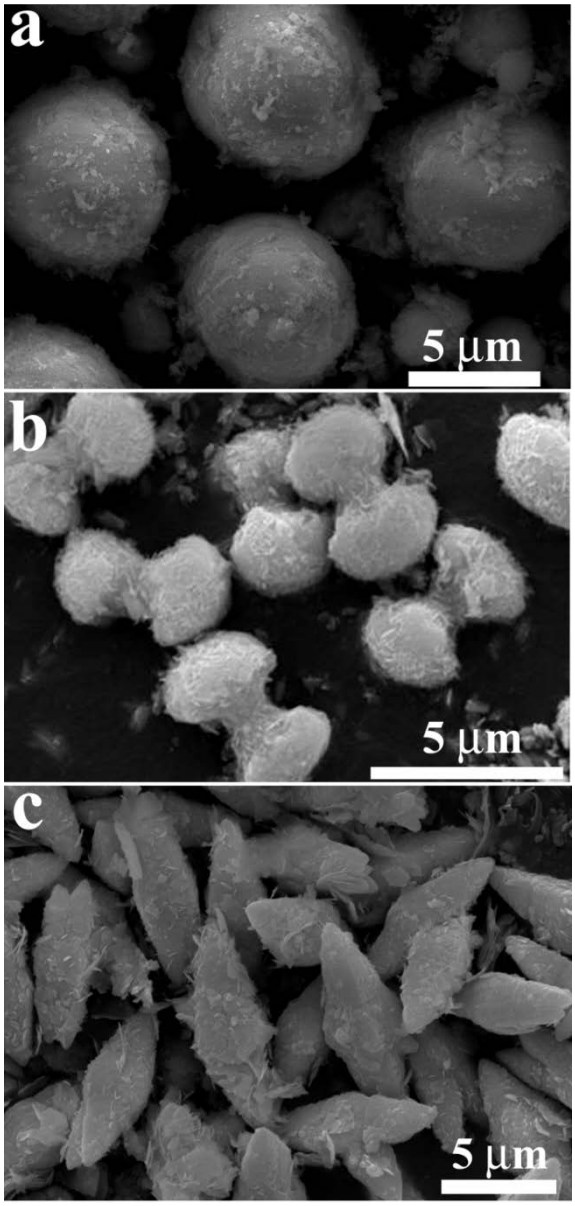

Fig. 4 SEM images of (a) CDs@$CaWO_4$: Yb^{3+}, Er^{3+}, (b) CDs@$SrWO_4$: Yb^{3+}, Er^{3+} and (c) CDs@$BaWO_4$: Yb^{3+}, Er^{3+} composites.

composed of uneven microspheres with diameter of about 7 μm (Fig. 4a), which is slightly larger than that of $CaWO_4$: Yb^{3+}, Er^{3+} samples. It can be seen that there are a lot of nanosheets on the surface of dumbbell-like CDs@$SrWO_4$: Yb^{3+}, Er^{3+} (Fig. 4b) and CDs@$BaWO_4$: Yb^{3+}, Er^{3+} composites (Fig. 4c). To further investigate the surface microstructure of CDs@AWO_4: Yb^{3+}, Er^{3+} samples, Fig. 5 (a, c, e) show the low-magnification TEM images of CDs@$CaWO_4$: Yb^{3+}, Er^{3+}, CDs@$SrWO_4$: Yb^{3+}, Er^{3+} and CDs@$BaWO_4$: Yb^{3+}, Er^{3+} composites, and the morphologies of these three samples are microsphere, dumbbell and bipyramid, respectively. The high-magnification TEM images taken at the border of a single microsphere, dumbbell and bipyramid are shown in Fig. 5 (b, d, f), as denoted by red oval in Fig. 5 (a, c, e). It indicates that the surface of these three CDs@AWO_4: Yb^{3+}, Er^{3+} (A = Ca, Sr, Ba) composites is composed of numerous disordered nanosheets. However, it can be clearly observed that the amount of nanosheets on the surface of CDs@$CaWO_4$: Yb^{3+}, Er^{3+} composites (Fig. 5a) is slightly decreased in contrast to $CaWO_4$: Yb^{3+}, Er^{3+} sample (Fig. 3a).

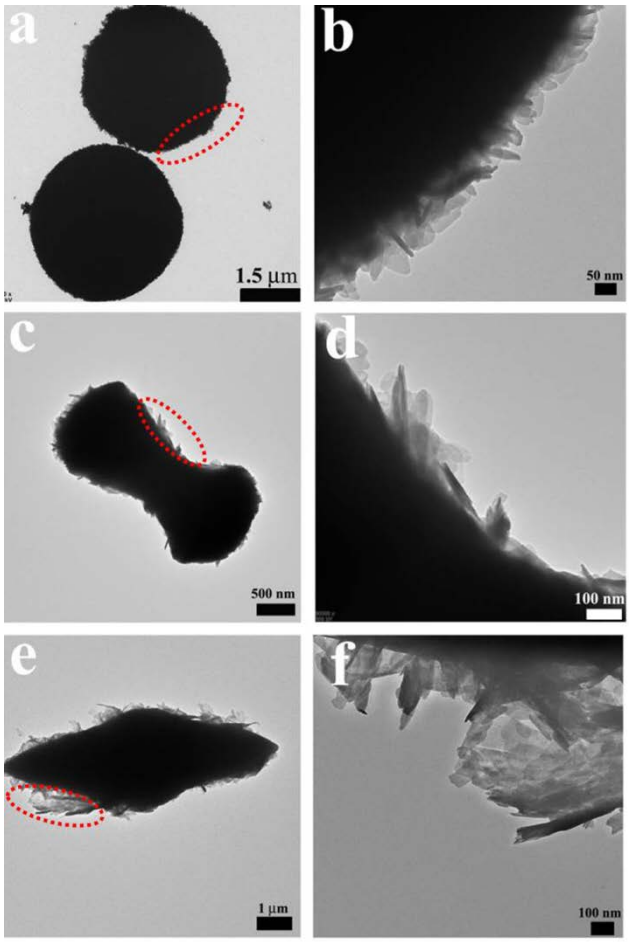

Fig. 5 The low- and high-magnification TEM images of (a, b) CDs@$CaWO_4$: Yb^{3+}, Er^{3+}, (c, d) CDs@$SrWO_4$: Yb^{3+}, Er^{3+} and (e, f) CDs@$BaWO_4$: Yb^{3+}, Er^{3+} composites.

To investigate the combination of CDs with AWO_4: Yb^{3+}, Er^{3+}, the chemical compositions of the representative CDs@$SrWO_4$: Yb^{3+}, Er^{3+} composites were analyzed by XPS spectra, as shown in Fig. 6. The XPS spectrum (Fig. 6a) shows the presence of O, N, C, Yb, Er, Sr and W elements. From the corresponding high-resolution XPS spectra, it can be seen that the peaks at 530.65 eV can be assigned to the binding energy of O 1s (Fig. 6b). The Yb 4d and Er 4d peaks (Fig. 6e) can be observed at 186.08 and 168 eV, respectively. The result well matches the previously observed peak features of Yb 4d and Er 4d.[46,47] The high-resolution XPS spectrum of Sr 3d (Fig. 6f) has two peaks: the peak around 133.1 eV corresponds to Sr 3d, and the other peak

at 134.6 eV is a satellite peak.[48] The peaks at 35.25 and 37.42 eV (Fig. 6g) are assigned to W $4f_{2/7}$ and W $4f_{2/5}$,[49] respectively. In addition, the peaks at 399.9 eV and 284.6 eV are detected, corresponding to N 1s (Fig. 6c) and C 1s (Fig. 6d) of CDs.[50] The XPS results provide a clear evidence that the CDs can be successfully combined with $SrWO_4$: Yb^{3+}, Er^{3+} to form CDs@$SrWO_4$: Yb^{3+}, Er^{3+} composites.

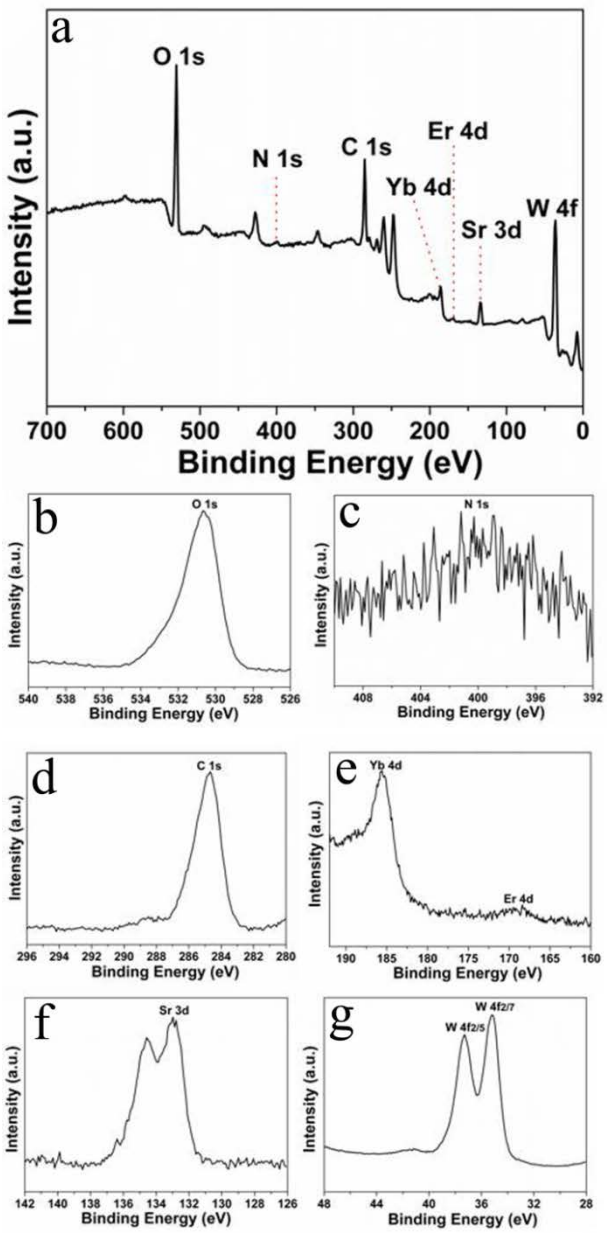

Fig. 6 (a) XPS spectrum of CDs@$SrWO_4$: Yb^{3+}, Er^{3+} and the corresponding high-resolution XPS spectra of (b) O 1s, (c) N 1s, (d) C 1s, (e) Yb 4d and Er 4d, (f) Sr 3d and (g) W 4f.

To further confirm the combination of CDs with AWO_4: Yb^{3+}, Er^{3+} samples, the PL emission spectra of CDs aqueous solution, the representative CDs@$SrWO_4$: Yb^{3+}, Er^{3+} composites and $SrWO_4$: Yb^{3+}, Er^{3+} dumbbells were studied and compared upon CDs excitation (λ_{ex} = 370 nm), as shown in Fig. 7. The emission spectrum of CDs solution shows a strong and broad emission band with peak at 455 nm (black line). The luminescence photograph of CDs solution exhibited a bright blue light by naked eyes under the excitation of 365 nm UV light, as shown in Fig. S3. For CDs@$SrWO_4$: Yb^{3+}, Er^{3+} composites, the spectrum shows a broad emission band centered at 425 nm (red line), similar to the emission band of CDs aqueous solution (black line), except that the peak position has a certain blue shift. This might be due to the interaction between CDs and $SrWO_4$: Yb^{3+}, Er^{3+} in CDs@$SrWO_4$: Yb^{3+}, Er^{3+} composites. For comparation, the emission spectrum (blue line) of $SrWO_4$: Yb^{3+}, Er^{3+} dumbbells has no emission band of CDs under the same excitation conditions. The PL results for CDs@$CaWO_4$: Yb^{3+}, Er^{3+} composites and $CaWO_4$: Yb^{3+}, Er^{3+} microspheres, CDs@$BaWO_4$: Yb^{3+}, Er^{3+} composites and $BaWO_4$: Yb^{3+}, Er^{3+} bipyramids systems are similar to that of CDs@$SrWO_4$: Yb^{3+}, Er^{3+} composites and $SrWO_4$: Yb^{3+}, Er^{3+} dumbbells system. This also indirectly indicates that the CDs can be successfully combined with AWO_4: Yb^{3+}, Er^{3+} samples to form CDs@AWO_4: Yb^{3+}, Er^{3+} composites.

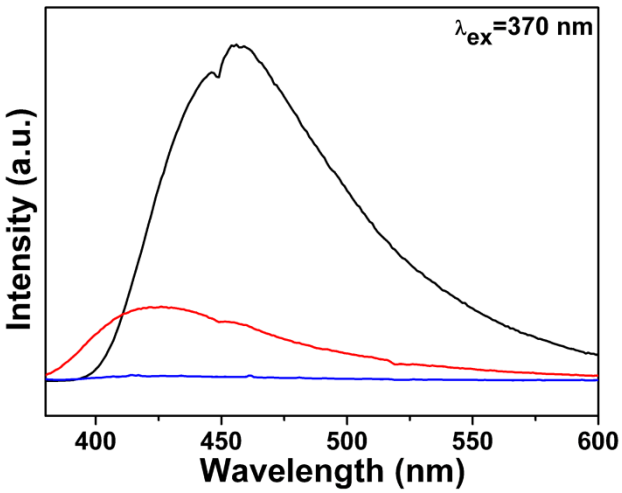

Fig. 7 PL emission spectra of CDs aqueous solution (black line), CDs@$SrWO_4$: Yb^{3+}, Er^{3+} composites (red line) and $SrWO_4$: Yb^{3+}, Er^{3+} dumbbells (blue line) under the excitation of 370 nm UV light.

3.3. UC luminescence enhancement effect through combination of CDs

The UC emission spectra of AWO_4: Yb^{3+}, Er^{3+} (A = Ca, Sr, Ba) samples and CDs@AWO_4: Yb^{3+}, Er^{3+} composites under a 980 nm laser excitation are shown in Fig. 8. It can be observed that the emission spectra of all samples exhibit two green emission bands and a red emission band of Er^{3+}. The green emission band between 500 and 540 nm is attributed to $^2H_{11/2}$–$^4I_{15/2}$ transitions, and the other one from 540 to 580 nm is assigned to $^4S_{3/2}$ –$^4I_{15/2}$ transitions, and the red emission band located at about 640–680 nm belongs to $^4F_{9/2}$–$^4I_{15/2}$ transitions. Compared to AWO_4: Yb^{3+}, Er^{3+} (A = Ca, Sr, Ba) samples (black line), the UC emission intensity of CDs@AWO_4: Yb^{3+}, Er^{3+} composites (red line) is prominently enhanced after

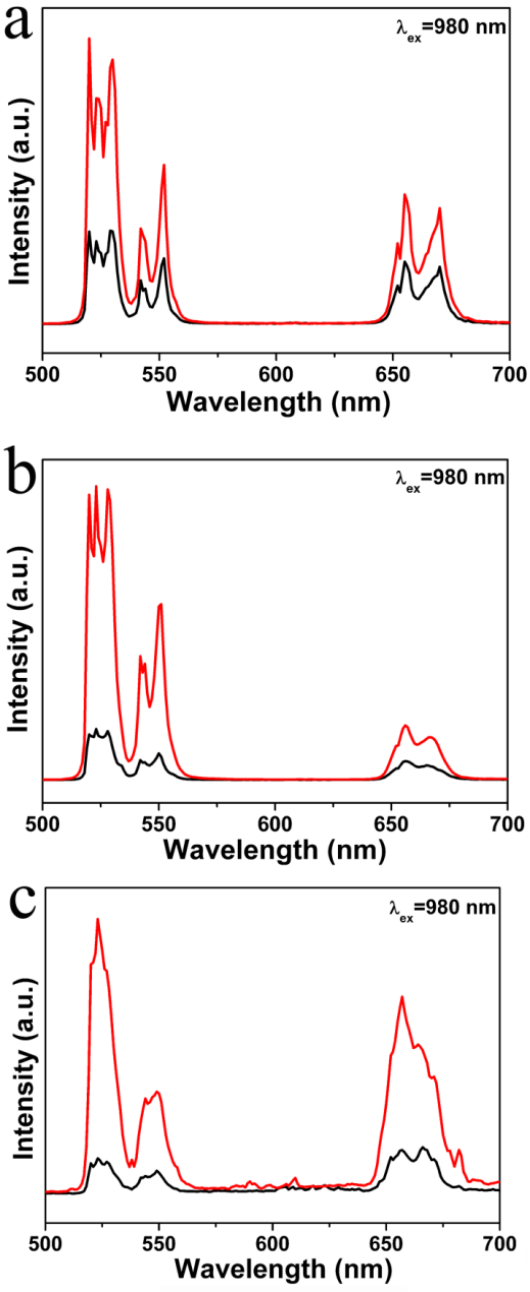

Fig. 8 UC emission spectra of (a) $CaWO_4$: Yb^{3+}, Er^{3+} and CDs@$CaWO_4$: Yb^{3+}, Er^{3+}, (b) $SrWO_4$: Yb^{3+}, Er^{3+} and CDs@$SrWO_4$: Yb^{3+}, Er^{3+}, (c) $BaWO_4$: Yb^{3+}, Er^{3+} and CDs@$BaWO_4$: Yb^{3+}, Er^{3+} under the excitation of 980 nm laser (Black and red lines represent before and after combination with CDs, respectively).

combinating with CDs. Fig. 8a shows the UC emission spectra of $CaWO_4$: Yb^{3+}, Er^{3+} and CDs@$CaWO_4$: Yb^{3+}, Er^{3+} composites, and the emission intensity of CDs@$CaWO_4$: Yb^{3+}, Er^{3+} composites is more than three folds higher than that of $CaWO_4$: Yb^{3+}, Er^{3+} microspheres in green emission band, and increases two folds in red emission band. The emission intensity of CDs@$SrWO_4$: Yb^{3+}, Er^{3+} composites is six and three times stronger than that of $SrWO_4$: Yb^{3+}, Er^{3+} dumbbells (Fig. 8b) in green and red emission band, respectively. The CDs@$BaWO_4$: Yb^{3+}, Er^{3+} composites have seven and four folds enhanced UC luminescence in contrast to $BaWO_4$: Yb^{3+}, Er^{3+} bipyramids in green and red emission areas, as shown in Fig. 8c.

3.4. UC luminescence enhanced mechanism

The proposed possible UC luminescence enhancement mechanism in CDs@AWO_4: Yb^{3+}, Er^{3+} system is schematically depicted in Fig. 9. Firstly, the sensitization process is formed through the Yb^{3+}–WO_4^{2-} system, and it includes the ground state absorption (GSA) and excited state absorption (ESA) processes.[51] The ground state of Yb^{3+}–WO_4^{2-} system is marked by [$^2F_{7/2}$, $^1A_1$], the intermediate excited state by [$^2F_{5/2}$, $^1A_1$], and the correlative higher excited states by [$^2F_{7/2}$, $^1E(^1T_1)$], [$^2F_{7/2}$, $^1E(^1T_2)$] and [$^2F_{7/2}$, $^1B(^1T_2)$], respectively.[52] The Yb^{3+}–WO_4^{2-} system is excited to the [$^2F_{7/2}$, $^1B(^1T_2)$] level by GSA ([$^2F_{7/2}$, $^1A_1$] → [$^2F_{5/2}$, $^1A_1$]) and ESA ([$^2F_{5/2}$, $^1A_1$] → [$^2F_{7/2}$, $^1B(^1T_2)$]). The excited energy at [$^2F_{7/2}$, $^1B(^1T_2)$] level could either transfer to [$^2F_{7/2}$, $^1E(^1T_2)$] level through non-radiative (NR) transition process, which might result in the low UC luminescence efficiency of Yb^{3+} and Er^{3+} co-doped tungstates. At the same time, the excited energy at [$^2F_{7/2}$, $^1B(^1T_2)$] level could be effectively captured by the energy level of CDs, and then transferred to [$^2F_{7/2}$, $^1E(^1T_2)$] energy level, which might effectively reduce the loss of non-radiative transitions from higher [$^2F_{7/2}$, $^1B(^1T_2)$] energy level to the lower [$^2F_{7/2}$, $^1E(^1T_2)$] energy level in the Yb^{3+}–WO_4^{2-} system. This will lead to increased population in [$^2F_{7/2}$, $^1E(^1T_2)$] energy level. The $^4F_{7/2}$ energy level of Er^{3+} ions can be populated through energy transfer process (ET) from [$^2F_{7/2}$, $^1E(^1T_2)$] state of the Yb^{3+}–WO_4^{2-} system to the $^4F_{7/2}$ energy level of Er^{3+}. And then, the two relatively stable levels of $^2H_{11/2}$ and $^4S_{3/2}$ are populated by the non-radiative transition from $^4F_{7/2}$ to the $^2H_{11/2}$ and $^4S_{3/2}$ lower levels. Finally, the $^2H_{11/2}$–$^4I_{15/2}$ and $^4S_{3/2}$–$^4I_{15/2}$ transitions of Er^{3+} will produce

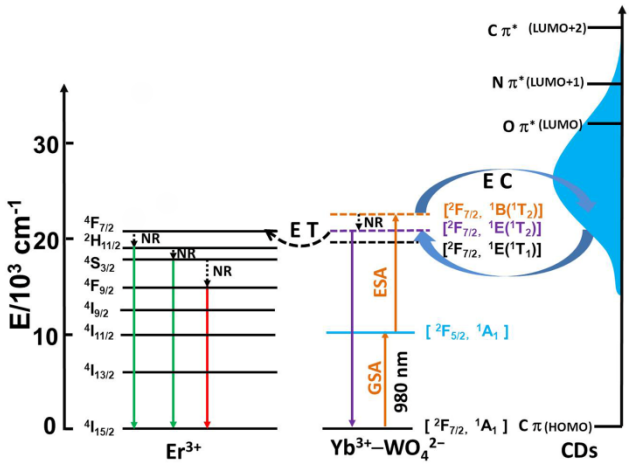

Fig. 9 Schematic diagram of UC luminescence enhancement mechanism in CDs@AWO_4: Yb^{3+}, Er^{3+} (A = Ca, Sr, Ba) system under 980 nm laser excitation (ET: energy transfer; EC: energy capture; NR: non-radiative).

enhanced green emission processes. For the red UC emission, the $^4F_{9/2}$ energy level can be populated by further non-radiative transition from $^4S_{3/2}$ to $^4F_{9/2}$, and the increased red UC emission corresponding to $^4F_{9/2}$–$^4I_{15/2}$ transitions of Er^{3+} can be observed.

4. Conclusions

In summary, UC luminescence AWO_4: Yb^{3+}, Er^{3+} (A = Ca, Sr, Ba) materials were successfully synthesized by a simple hydrothermal method. The as-prepared AWO_4: Yb^{3+}, Er^{3+} samples have a body-centered scheelite structure with various morphologies including microspheres ($CaWO_4$: Yb^{3+}, Er^{3+}), dumbbells ($SrWO_4$: Yb^{3+}, Er^{3+}) and bipyramids ($BaWO_4$: Yb^{3+}, Er^{3+}). The UC luminescence of AWO_4: Yb^{3+}, Er^{3+} samples can be prominently enhanced through combining with CDs to form CDs@AWO_4: Yb^{3+}, Er^{3+} composites. The mechanism behind observing UC luminescence enhancement is probably attributed to the energy capture by CDs, which can effectively reduce the losses of non-radiative transitions from higher energy levels to the lower excited energy level. The investigation develops a novel and feasible strategy to improve the UC luminescence property not only for tungstates but also for other host systems.

Acknowledgements

This work is financially supported by the National Natural Science Foundation of China (no. 51572303), the Innovation Scientists and Technicians Troop Construction Projects of Henan Province (no. 2013259), and Hong Kong RGC GRF (No. PolyU 153281/16P).

References

1 W. Feng, C. M. Han and F. Y. Li, *Adv. Mater.*, 2013, **25**, 5287–5303.
2 F. Wang and X. G. Liu, *Chem. Soc. Rev.*, 2009, **38**, 976–989.
3 F. Auzel, *Chem. Rev.*, 2004, **104**, 139–174.
4 M. M. Shang, C. X. Li and J. Lin, *Chem. Soc. Rev.*, 2014, **43**, 1372–1386.
5 G. B. Shan, H. Assaaoudi and G. P. Demopoulos, *ACS Appl. Mater. Interfaces,* 2011, **3**, 3239–3243.
6 F. Wang and X. G. Liu, *J. Am. Chem. Soc.*, 2008, **130**, 5642–5643.
7 Z. Yin, D. L. Zhou, W. Xu, S. B. Cui, X. Chen, H. Wang, S. H. Xu, and H. W. Song, *ACS Appl. Mater. Interfaces*, 2016, **8**, 11667–11674.
8 M. Saboktakin, X. C. Ye, U. K. Chettiar, N. Engheta, C. B. Murray and C. R. Kagan, *ACS Nano*, 2013, **7**, 7186–7192.
9 N. J. Greybush, M. Saboktakin, X. C. Ye, C. D. Giovampaola, S. J. Oh, N. E. Berry, N. Engheta, C. B. Murray and C. R. Kagan, *ACS Nano*, 2014, **8**, 9482–9491.
10 D. W. Lu, S. K. Cho, S. Ahn, L. Brun, C. J. Summers and W. Park, *ACS Nano*, 2014, **8** ,7780–7792.
11 G. B. Shan and G. P. Demopoulos, *Adv. Mater.*, 2010, **22**, 4373–4377.
12 J. H. Wu, J. L. Wang, J. M. Lin, Z. Lan, Q. W. Tang, M. L. Huang, Y. F. Huang, L. Q. Fan, Q. B. Li and Z. Y. Tang, *Adv. Energy Mater.*, 2012, **2**, 78–81.
13 H. Q. Wang, M. Batentschuk, A. Osvet, L. Pinna and C. J. Brabec, *Adv. Mater.*, 2011, **23**, 2675–2680.
14 S. L. Gai, C. X. Li, P. P. Yang and J. Lin, *Chem. Rev.*, 2014, **114**, 2343−2389.
15 L. P. Li, Y. G. Su and G. S. Li, *Appl. Phys. Lett.*, 2007, **90**, 054105.
16 S. H. Yu, B. Liu, M. S. Mo, J. H. Huang, X. M. Liu and Y. T. Qian, *Adv. Funct. Mater.*, 2003, **13**, 639–647.
17 A. A. Kaminskii, H. J. Eichler, K. I. Ueda, N. V. Klassen, B. S. Redkin, L. E. Li, J. Findeisen, D. Jaque and R. Balda, *Appl. Opt.*, 1999, **38**, 4533–4547.
18 Q. Zhang, W. T. Yao, X. Chen, L. Zhu, Y. Fu, G. Zhang, L. Sheng and S. H. Yu, *Cryst. Growth Des.*, 2007, **7**, 1423–1431.
19 L. Sun, Q. Guo, X. Wu, S. Luo, W. Pan, K. Huang, J. Lu, L. Ren, M. Cao and C. Hu, *J. Phys. Chem. C*, 2007, **111**, 532–537.
20 W. S. Cho, M. Yashima, M. Kakihana, A. Kudo, T. Sakata and M. Yoshimura, *Appl. Phys. Lett.*, 1995, **66**, 1027–1029.
21 R. F. Gonçalves, L. S. Cavalcante, I. C. Nogueira, E. Longo, M. J. Godinho, J. C. Sczancoski, V. R. Mastelaro, I. M. Pinatti, I. L. V. Rosa and A. P. Marques, *CrystEngComm*, 2015, **17**, 1654–1666.
22 Y. G. Su, L. P. Li and G. S. Li, *Chem. Mater.*, 2008, **20**, 6060–6067.
23 S. Mahlik, E. Cavalli, M. Amer and P. Boutinaud, *Phys. Chem. Chem. Phys.*, 2015, **17**, 32341–32346.
24 Z. Y. Hou, C. X. Li, J. Yang, H. Z. Lian, P. P. Yang, R. T. Chai, Z. Y. Cheng and J. Lin, *J. Mater. Chem.*, 2009, **19**, 2737–2746.
25 W. X. Wang, P. P. Yang, Z. Y. Cheng, Z. Y. Hou, C. X. Li and J. Lin, *ACS Appl. Mater. Interfaces*, 2011, **3**, 3921–3928.
26 S. P. Culver and R. L. Brutchey, *Dalton Trans.*, 2016, **45**, 18069–18073.
27 B. Y. Xu, X. Cao, G. F. Wang, Y. Li, Y. P. Wang and J. M. Su, *Dalton Trans.*, 2014, **43**, 11493–11501.
28 Maheshwary, B. P. Singh, J. Singh and R. A. Singh, *RSC Adv.*, 2014, **4**, 32605–32621.
29 G. H. Jia, C. F. Wang and S. Q. Xu, *J. Phys. Chem. C*, 2010, **114**, 17905–17913.
30 Y. P. Wang, Y. Qu, K. Pan, G. F. Wang and Y. D. Li, *Chem. Commun.*, 2016, **52**, 11124–11126.
31 P. Jena, S. K. Gupta, N. K. Verma, A. K. Singh and R. M. Kadam, *New J. Chem.*, 2017, **41**, 8947–8958.
32 W. Xu, Z. G. Zhang and W. W. Cao, *Opt. Lett.*, 2012, **37**, 4865–4867.
33 X. N. Chai, J. Li, Y. Zhang, X. S. Wang, Y. X. Li and X. Yao, *RSC Adv.*, 2016, **6**, 64072–64078.
34 J. Liu, A. M. Kaczmarek, J. Billet, I. V. Driessche and R. V. Deun, *Dalton Trans.*, 2016, **45**, 12094–12102.
35 F. Wang, Y. Han, C. S. Lim, Y. Lu, J. Wang, J. Xu, H. Chen, C. Zhang, M. Hong and X. Liu, *Nature*, 2010, **463**, 1061−1065.
36 G. S. Yi and G. M. Chow, *Chem. Mater.*, 2007, **19**, 341−343.
37 F. Vetrone, R. Naccache, V. Mahalingam, C. G. Morgan and J. A. Capobianco, *Adv. Funct. Mater.*, 2009, **19**, 2924−2929.
38 G. X. Bai, M. K. Tsang and J. H. Hao, *Adv. Funct. Mater.*, 2016, **26**, 6330−6350.
39 S. J. Zhu, Q. N. Meng, L. Wang, J. H. Zhang, Y. B. Song, H. Jin, K. Zhang, H. C. Sun, H. Y. Wang and B. Yang, *Angew. Chem. Int. Ed.*, 2013, **52**, 3953–3957.
40 A. Pandey, V. K. Rai, V. Kumar and H. C. Swart, *Sens. Actuators B*, 2015, **209**, 352–358.
41 G. X. Zhang, R. Jia and Q. S. Wu, *Mater. Sci. Eng: B*, 2006, **128**, 254–259.
42 M. A. M. A. Maurera, A. G. Souza, L. E. B. Soledade, F. M. Pontes, E. Longo, E. R. Leite, J. A. Varela, *Mater. Lett.*, 2004, **58**, 727–732.
43 P. Goel, M. K. Gupta, R. Mittal, S. Rols, S. N. Achary, A. K. Tyagi and S. L. Chaplot, *Phys. Rev. B*, 2015, **91**, 094304.
44 G. H. Jia, C. F. Wang and S. Q. Xu, *J. Phys. Chem. C*, 2010, **114**, 17905–17913.
45 H. T. Shi, X. H. Wang, N. N. Zhao, L. M. Qi and J. M. Ma, *J. Phys. Chem. B*, 2006, **110**, 748–753.
46 P. Ramasamy, P. Chandra, S. W. Rhee and J. Kim, *Nanoscale*, 2013, **5**, 8711–8717.
47 G. X. Bai, S. G. Yuan, Y. D. Zhao, Z. B. Yang, S. K. Choi, Y. Chai, S. F. Yu, S. P. Lau and J. H. Hao, *Adv. Mater.*, 2016, **28**, 7472–7477.
48 F. Zhang, M. Y. Sfeir, J. A. Misewich and S. S. Wong, *Chem. Mater.*, 2008, **20**, 5500–5512.

49 B. V. Kumar, M. D. Prasad and M. Vithal, *Mater. Lett.*, 2015, **152**, 200–202.
50 S. K. Bhunia, N. Pradhan, N. R. Jana, *ACS Appl. Mater. Interfaces*, 2014, **6**, 7672–7679.
51 B. Dong, B. S. Cao, Y. Y. He, Z. Liu, Z. P. Li and Z. Q. Feng, *Adv. Mater.*, 2012, **24**, 1987–1993.
52 X. X. Yang, Z. L. Fu, Y. M. Yang, C. P. Zhang, Z. J. Wu and T. Q. Sheng, *J. Am. Ceram. Soc.*, 2015, **98**, 2595–2600.

